PAPER

Check for updates

Triangular-shaped Cu–Zn–In–Se-based nanocrystals with narrow near infrared photoluminescence†

Ankita Bora,[a] Ningyuan Fu, [iD][a] Avijit Saha,[a] Anatol Prudnikau,[a] René Hübner, [iD][b] Houman Bahmani Jalali, [iD][c] Francesco Di Stasio, [iD][c] Nikolai Gaponik [iD] ‡[a] and Vladimir Lesnyak [iD] *[a]

Tunable optical properties exhibited by semiconductor nanocrystals (NCs) in the near infrared (NIR) spectral region are of particular interest in various applications, such as telecommunications, bioimaging, photodetection, photovoltaics, *etc*. While lead and mercury chalcogenide NCs do exhibit exemplary optical properties in the NIR, Cu–In–Se (CISe)-based NCs are a suitable environment-friendly alternative to these toxic materials. Several reports of NIR-emitting (quasi)spherical CISe NCs have been published, but their more complex-shaped counterparts remain rather less explored. The emerging anisotropic nanomaterials have gained significant interest owing to their unique optical properties arising due to their specific shape. While several examples of non-spherical Cu–In–S-based NCs have been reported, examples of CISe-based anisotropic NCs are rather scarce, and those with intensive photoluminescence (PL) are not yet developed. In this work, we present a one-pot approach to synthesize quaternary Cu–Zn–In–Se (CZISe) triangular NCs with intensive PL in the NIR region. The NCs synthesized exhibit tetragonal crystal structure and, depending on the reaction conditions, are single triangular particles or stacks of triangular blocks of varied lateral sizes but rather uniform thickness. The synthesis involves the formation of In_2Se_3 seeds with subsequent incorporation of copper and growth of triangular CISe NCs, followed by the incorporation of zinc and the growth of a ZnS shell. Importantly, the PL band widths of the final core/shell heterostructured NCs are narrow, down to 102 meV, which is a rarely observed characteristic for this class of materials and can be attributed to their anisotropic shape and the absence of thickness and compositional inhomogeneities of their building blocks. The PL of the CZISe/ZnS NCs can be tuned in the range of 1082–1218 nm reaching a quantum yield of up to 40% by varying their size and composition. To the best of our knowledge, this is the farthest and the narrowest PL achieved for CISe-based NCs so far, which widens application perspectives of this material in NIR LEDs, bioimaging, and photovoltaics.

[a]*Physical Chemistry, TU Dresden, Zellescher Weg 19, 01069 Dresden, Germany. E-mail: vladimir.lesnyak@tu-dresden.de*
[b]*Institute of Ion Beam Physics and Materials Research, Helmholtz-Zentrum Dresden-Rossendorf e.V., Bautzner Landstrasse 400, 01328 Dresden, Germany*
[c]*Photonic Nanomaterials, Istituto Italiano di Tecnologia, via Morego 30, 16163 Genova, Italy*

Introduction

Tunable optical properties in the near infrared (NIR) window of 1300–1600 nm are of particular interest in telecommunications,[1] while biological windows spanning the NIR emission wavelength ranges of 700–900 nm, 1000–1350 nm, and 1150–1870 nm are attractive for bioimaging.[2,3] Additionally, the NIR window of 800–2000 nm is important in photovoltaics.[1] Due to a narrow bulk band gap and high optical efficiencies, lead and mercury chalcogenide nanocrystals (NCs) have been proven as candidates of choice for a wide range of NIR-based applications.[4–8] However, the presence of toxic elements poses a major setback in their widespread use, particularly in those applications involving exposure to biological environments. This has led to the development of I–III–VI-

based semiconductor NCs as a less-toxic earth-abundant metal-containing alternative with potential as NIR emitters, making them a suitable replacement as fluorophores in various applications.[4,9,10] Among them, Cu–In–Se (CISe)-based NCs with a quite narrow bulk band gap of 1.04 eV and a large exciton Bohr radius of 10.6 nm are an interesting and less-studied member of this class of semiconductors.[9] While reports of NIR-emitting CISe NCs are abundant, their optical activity is limited to 1100–1200 nm and pushing it to even longer wavelengths would unlock a plethora of applications.[11–16] Thus, CISe NCs emitting at as far as 1200 nm but with a very low photoluminescence quantum yield (PLQY) of 0.1% were reported.[9] Furthermore, approx. 5 nm-sized Cu–Zn–In–Se (CZISe) NCs exhibiting composition tuneable PL in the range of 980–1060 nm with 20% PLQY have been developed recently.[10] Therefore, there is still scope for improvement of the PL tuneability and optical efficiency of CISe-based NCs in the NIR range, which needs to be explored.

Recent studies on two-dimensional (2D) semiconductor NCs have shown that they exhibit unique properties, which are attributed to their anisotropic shape.[17–23] Atomically flat nanoplatelets (NPLs) or nanosheets have thicknesses, which are much smaller than the corresponding exciton Bohr radius, while having larger lateral dimensions, leading to strong quantum confinement in only one direction, i.e., within their thickness.[24] Unique properties of these materials include exceptionally narrow PL spectra, enhanced optical absorption, suppressed Auger-recombination, and giant oscillator strength.[21,25,26] Noteworthy, the research on 2D NCs has mostly been done on binary metal chalcogenides, including toxic Cd[21,27,28] and Pb[23,25,29] compounds and very scarcely explored in the case of multicomponent I–III–VI-based NCs. It is therefore reasonable to extend the study of anisotropic properties to this class of semiconductor NCs as well, which might also reveal interesting optical features that are not in alignment with the much more explored (quasi)spherical NCs. Cu–In–S (CIS)-based NCs are most studied in the I–III–VI group of 2D materials, various reports of which are present in the literature.[17,24,30–33] However, the selenide counterparts of this class of materials have not been rigorously explored, with limited previous reports. For instance, Zhong et al. reported the synthesis of hexagonal CISe NPLs using dodecanethiol (DDT) as a ligand and 1-octadecene (ODE) as a non-coordinating solvent.[34] They obtained CISe NCs at a moderate temperature of 180 °C, while at an elevated temperature of 210 °C and a long reaction time of 3 h, hexagonal plates with sharp edges were grown. A mixture of triangular, hexagonal, and disk-like CISe NPLs was synthesized by Tang et al. by a one-pot approach using salts of Cu, Se powder, and oleylamine (OlAm).[35] The synthesis of ultrathin CISe nanosheets and NPLs derived via cation exchange (CE) from 2D $Cu_{2-x}Se$ using a dodecaneselenol precursor was reported by Berends et al.[36] A variation of reaction parameters enabled them to control the shape of the 2D $Cu_{2-x}Se$ NCs, which then served as templates for the incorporation of In^{3+} while preserving their morphology. Bi et al. reported the synthesis of ultrathin CISe NPLs

via CE using self-sacrificial CuSe templates.[37] As follows from their characterization details, none of these examples exhibited highly intensive PL and, to the best of our knowledge, NIR-emitting CISe-based 2D NCs have not been reported so far. Thus, the development of synthetic strategies for anisotropic CISe-based NCs emitting in the NIR range is an open research topic which should be addressed. In addition, it is well-established that the incorporation of Zn in CIS(Se)-based NCs and the deposition of a ZnS shell help in augmenting their PLQY and, therefore, exploring quaternary anisotropic CZISe NCs as well as their coating with a ZnS shell are also of interest.[24,38]

While direct synthesis has been used to obtain I–III–VI-based NCs, more control over the formation of these multicomponent NCs is offered by the alternative CE or template synthesis pathway.[39–41] Direct synthesis is advantageous in terms of simplicity and fast reaction, however, its major drawback for the growth of complex-shaped NCs is usually their irregular morphology and broad size distribution.[24] Therefore, the CE pathway, wherein guest cations are introduced into the crystal structure of a binary chalcogenide (pre-synthesized via the direct method) by replacing the host cations or/and filling up the vacancies, serves as a more suitable method.[39] It offers a better control over the formation of multicomponent ternary/quaternary NCs by eliminating unwanted reactions between multiple precursors involved in the direct synthesis.[9,38,40,42] The main challenge of realizing anisotropic morphologies using the CE pathway is to retain the shape of the template NCs throughout the reaction, which is possible to achieve by careful optimization of the reaction parameters.[25] In most cases, such CE strategy for the synthesis of I–III–VI-based NCs starts with a binary copper chalcogenide which serves as a template for further incorporation of the guest cations. For example, pre-synthesized $Cu_{2-x}Se_yS_{1-y}$ NPLs served as templates for subsequent partial CE with Zn^{2+} or/and Sn^{4+} ions, leading to the formation of 2D Cu–Zn–Se–S, Cu–Sn–Se–S, and Cu–Zn–Sn–Se–S NCs with controlled composition.[33] Starting from ultrathin covellite CuS NPLs, Wu et al. synthesized quite monodisperse ternary CIS and quaternary $CuIn_xGa_{1-x}S_2$ and Cu_2ZnSnS_4 NPLs at high temperatures.[31] Similar CuS NPLs were employed as templates by Lox et al. in the synthesis of alloyed Cu–Zn–In–S (CZIS) NPLs and cookie-shaped CZIS/ZnS NPLs.[24] Shamraienko et al. synthesized binary PbSe, HgSe, ZnSe, SnSe, and quaternary Cu–Zn–Sn–Se nanosheets starting from thin CuSe nanosheets[43] followed by either partial or complete exchange of the host cations.[44]

Typically, ternary/quaternary NCs are synthesized using the corresponding binary copper chalcogenides as templates.[36] As an alternative route, indium chalcogenide NCs can also act as host particles for partial exchange with Cu^+ ions, yielding CIS(Se)-based NCs.[45] Following this route, Chen et al. synthesized In_2S_3 NPLs which served as templates for the incorporation of copper at room temperature, leading to the formation of CIS NPLs.[46] They further employed these NPLs for the fabrication of dye-sensitized solar cells with a power conversion efficiency of 6.83%. Using a similar approach, Yuan et al. developed the synthesis of CIS and CZIS NPLs with intensive PL in the visible

range starting from 2D In_2S_3 host templates.[47] The synthesis of binary template In_2S_3 NPLs reported by Park et al.[48] provides a direction for its adoption to obtain similar In_2Se_3 NPLs. The difference in reactivities of S- and Se-precursors, however, necessitates the modification of the reaction conditions. Such In_2Se_3 NPLs could serve as a new template species for the further incorporation of incoming Cu^+ cations, resulting in anisotropic CISe-based NCs, which might exhibit interesting optoelectronic features.

In this work, we report the seed-mediated synthesis of ternary anisotropic CISe NCs followed by the incorporation of zinc ions, resulting in quaternary CZISe NCs with intensive PL in the NIR region, which can further be improved by growing a ZnS shell. As a starting point, In_2Se_3 seeds are synthesized first, followed by the formation of CISe seeds *via* the addition of a small amount of a Cu-precursor at room temperature. Thereafter, the anisotropic growth of these seeds is promoted by an increase in reaction temperature, leading to the formation of CISe NPLs. To enhance the PL intensity and to improve the stability of these NCs, Zn is incorporated in the subsequent step. The presence of a single amine in the synthesis leads to a stacked ligand arrangement, thereby resulting in triangular NPLs, which can further grow and form stacks upon increasing reaction temperature. In the final stage of the synthesis, anisotropic CZISe NCs are covered with a ZnS shell, resulting in a two-fold increase of their PLQY up to 40%. Thus, the as-synthesized NCs exhibit an intensive PL in the NIR range with very narrow PL bandwidths of 102–122 meV, as compared to broad PL spectra generally exhibited by I–III–VI-based NCs. The variation of different parameters, such as the NC composition and the temperature of the synthesis, allows for tuning of their optical properties. These NIR-emitting NCs are of particular interest in bioimaging due to their low toxic nature and environmentally benign composition.

Experimental section

Materials

Indium(III) chloride ($InCl_3$, 99.99%) and zinc 2-ethyl hexanoate (17–19% Zn) were purchased from Alfa Aesar. Selenium powder (Se, 99.99%), tetrakis (acetonitrile) copper(I) hexafluorophosphate ([$Cu(CH_3CN)_4$]PF_6, 97%), zinc acetate dihydrate ($Zn(OAc)_2 \cdot 2H_2O$, 98%), oleic acid (OlAc, 90%), 1-octadecene (ODE, 90%), oleylamine (OlAm, 70%), tetrachloroethylene (TCE, 99%), and dodecanethiol (DDT, 99%) were purchased from Sigma-Aldrich. Extra dry acetonitrile (99.9%) was purchased from Acros Organics. Toluene (≥99.8%) was purchased from Fischer Chemicals. Methanol (99.9%) was purchased from VWR.

Synthesis of In_2Se_3 seeds and nanosheets

The synthesis of In_2Se_3 nanosheets was adapted from the method reported by Park et al.[48] For the synthesis, first, an In-precursor was prepared by mixing 66.3 mg (0.3 mmol) of $InCl_3$ with 3 mL of OlAm inside a nitrogen-filled glovebox. This mixture was kept under vigorous shaking at room temperature until all $InCl_3$ was dissolved in OlAm. In parallel, the Se-precursor was prepared by dispersing 15.8 mg (0.2 mmol) of Se powder in 1 mL of OlAm by ultrasonication and then purging the mixture with nitrogen. 5 mL of OlAm were loaded into a 25 mL three-neck round-bottom flask equipped with a thermocouple and a magnetic stirrer and degassed for 30 min at room temperature. Thereafter, the flask was filled with nitrogen and the temperature was raised to 205 °C. When the temperature of 205 °C was attained, the Se suspension was injected into the flask. After approx. 10–12 min, the Se powder was dissolved in OlAm, forming a transparent orange solution. After the complete dissolution of the Se powder, the reaction mixture was cooled down to 115 °C and the In-precursor was swiftly injected, leading to a color change from orange to bright yellow. The reaction mixture was maintained at this temperature for 1 h to produce In_2Se_3 seeds. After 1 h, the mixture was further heated to 230 °C for 1 h to form In_2Se_3 nanosheets.

Synthesis of CISe NCs

For the synthesis of triangular CISe NCs, the above-mentioned steps for the synthesis of In_2Se_3 seeds were carried out. Simultaneously, a Cu-precursor was prepared inside the glovebox by dissolving 55.90 mg (0.15 mmol) of [$Cu(CH_3CN)_4$]PF_6 in 2 mL of acetonitrile at room temperature. After the synthesis of the In_2Se_3 seeds, the reaction mixture was cooled down to room temperature and 200 μL of the Cu-precursor were injected, leading to an immediate color change from yellow to brown. The reaction mixture was kept under stirring overnight, and on the next day, it was heated to a desired temperature for 1 h to promote the growth of CISe NCs. Herein, we annealed the reaction mixture at 215 °C, 230 °C, or 240 °C to obtain small-, medium-, and large-sized NCs, respectively. Subsequently, the reaction mixture was cooled down to room temperature and 1 mL of DDT (previously purged with nitrogen) was added. This mixture was further kept under stirring for 1 h. Aliquots of this mixture were taken, and NPLs were precipitated by adding methanol followed by centrifugation and redispersion in toluene. An additional purification step was carried out, and the obtained NCs were dispersed in 2 mL of toluene and stored for further characterization.

Synthesis of CZISe NCs

For the synthesis of CZISe NCs, 1080 μL (3 mmol) of zinc 2-ethylhexanoate were added to the as-synthesized CISe NCs followed by heating to 230 °C for 1 h. After 1 h, the reaction mixture was cooled down to room temperature and the NCs were precipitated by adding methanol and centrifuging at 5000 rpm. The supernatant was discarded, and the precipitate was redispersed in toluene and purified once again. Finally, the CZISe NCs were redispersed in 4 mL of toluene and stored in a refrigerator for further characterization.

Synthesis of CZISe/ZnS core/shell NCs

We continued the reaction after the CZISe NCs synthesis by growing a ZnS shell to form core/shell CZISe/ZnS NCs. Zinc precursor (zinc oleate) and sulfur precursor (S dissolved in ODE) were prepared following the literature procedure,[49] as described in the ESI.† The reaction temperature after the zinc incorporation was lowered to 200 °C, followed by a slow addition of 3 mL of the preheated zinc oleate and 2.4 mL of the sulfur precursor. The reaction mixture was then kept under continuous stirring for 1 h at the same temperature for the ZnS shell growth. Subsequently, the temperature was reduced to room temperature. All the samples were purified 2–3 times using a toluene/methanol (ratio 1 : 1) mixture, centrifuged at 5000 rpm for 3 min followed by redispersion of the obtained precipitate in toluene.

Transmission electron microscopy (TEM) imaging

TEM sample preparation included additional purification of the NCs by reprecipitation with methanol and dissolving in toluene to obtain a very dilute solution. The solution was drop-cast onto a carbon-coated copper grid with subsequent evaporation of the solvent. Conventional TEM imaging was carried out on a JEOL JEM 1400 microscope equipped with a thermionic gun (W filament) working at an accelerating voltage of 120 kV. High-resolution TEM imaging was performed on an image-C_s-corrected Titan 80–300 microscope operated at 300 kV. High-angle annular dark-field scanning TEM (HAADF-STEM) imaging and spectrum imaging analysis based on energy-dispersive X-ray spectroscopy (EDXS) were performed at 200 kV with a Talos F200X microscope equipped with an X-FEG electron source and a Super-X EDX detector system (FEI). Prior to (S)TEM analysis, the specimen mounted in a high-visibility low-background holder was placed for 2 s into a model 1020 Plasma Cleaner (Fischione) to remove potential contamination. For STEM-based analysis, the NC solution was drop-cast onto a carbon-coated Ni grid to avoid Cu fluorescence radiation.

Powder X-ray diffraction (XRD) analysis

All crude reaction mixtures were transferred inside the glovebox immediately after the synthesis and purified under inert gas for XRD measurements. The samples were prepared by drop-casting concentrated NC solutions onto a zero-background silicon wafer. XRD patterns were recorded on a Bruker D2 Phaser using a Cu source operating at 30 kV and 10 mA.

UV-Vis-NIR absorption spectroscopy

Samples were prepared by diluting dispersions of NCs in toluene. The absorption spectra were recorded on a Cary 60 UV-Vis and a Cary 5000 UV-Vis-NIR spectrophotometers (Varian) using 1 cm path length quartz cuvettes.

Photoluminescence measurements

The samples for PL measurements were prepared by dispersing the NCs in TCE. The PL spectra were recorded on a Fluorolog-3 spectrofluorometer (Horiba Jobin Yvon) using an excitation wavelength of 435 nm. For PLQY measurements, the NCs were dispersed in toluene and were characterized using an Edinburgh Instruments FLS900 fluorescence spectrometer equipped with an integrating sphere and a Xe lamp (λ_{ex} = 800 nm). All solutions were diluted to an optical density of approx. 0.1–0.15 at 800 nm. Time-resolved PL traces were acquired on the same device equipped with a TCSPC card and a pulsed laser diode for excitation.

Elemental analysis

The samples for inductively coupled plasma optical emission spectroscopy (ICP-OES) were prepared by decomposing the NCs in 2% aqua regia with subsequent dilution with Milli-Q water. The measurements were carried out on a PerkinElmer Optima 7000DV instrument with matrix-matched calibration standard solutions.

Results and discussion

Synthesis of In₂Se₃ nanosheets

In_2Se_3 nanosheets were synthesized using a modified procedure (see Fig. 1) reported by Park *et al.* for In_2S_3 nanosheets.[48] Different from the recipe, we employed 1.5 equivalents of In and 1 equivalent of Se (*i.e.* excess of indium) to consume all selenium reactive species before adding copper in order to avoid the formation of copper selenide byproduct particles. The reaction temperature was also altered to compensate for the difference in reactivity of the S- and Se-precursors. It has been observed that syntheses with Se-precursors typically require higher temperatures and longer reaction times than those involving S-precursors. Therefore, the temperature for In_2Se_3 seeds formation was raised to 115 °C and the temperature for subsequent NPL growth was raised to 230 °C. TEM imaging of the product revealed the formation of large nanosheets (see Fig. S1 in the ESI†). It should be noted that In_2Se_3 is a polymorphic material which exists in many crystal phases, three of which are the most common – α, β, and γ. Ambient conditions favor its crystallization into the layered α and β phases with either hexagonal or rhombohedral structure.[50–52] Hexagonal In_2Se_3 nanosheets crystallizing in the β phase, synthesized using a selenourea precursor and short aminonitriles as shape-controlling agents, were reported by Almeida *et al.*[53] For more detailed information, the synthesis of low-dimensional In_2Se_3 in different phases and its corresponding applications are discussed in the review by Li *et al.*[52] In our case, In_2Se_3 crystallizes in the α phase, as seen from the XRD pattern displayed in Fig. 2. Thus, the successful synthesis of In_2Se_3 nanosheets paved the way to the synthesis of anisotropic triangular CISe and CZISe NCs by using similar In_2Se_3 seeds.

Synthesis of triangular CISe, CZISe, and CZISe/ZnS NCs

The multistep one-pot synthesis method for heterostructured core/shell CZISe/ZnS NCs was inspired by the synthesis of CZIS
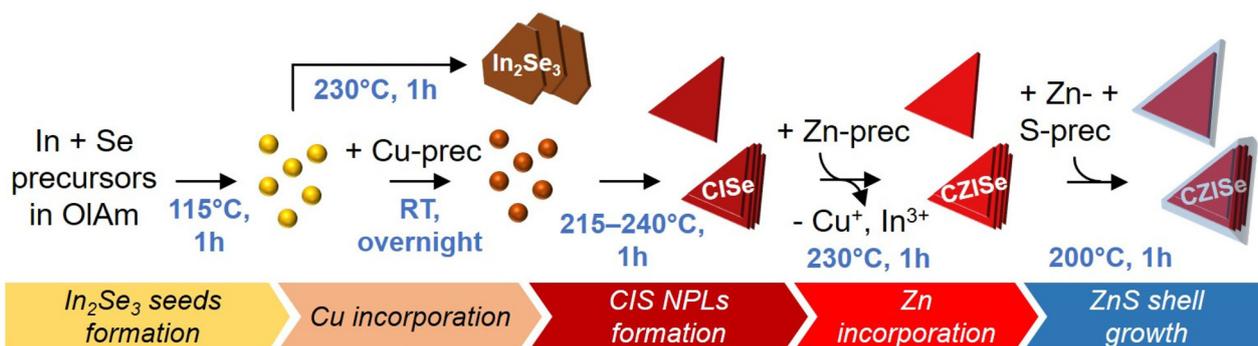
Fig. 1 Scheme of the synthesis of In_2Se_3 nanosheets, triangular CISe NCs, CZISe, and core/shell CZISe/ZnS NCs.
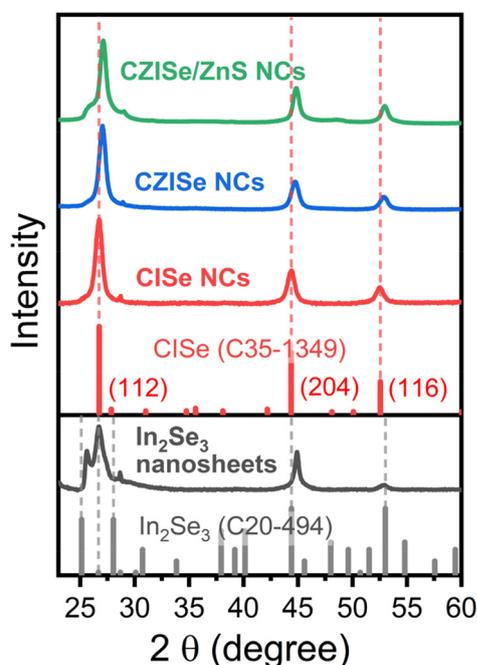

Fig. 2 XRD patterns of In_2Se_3 nanosheets, CISe, CZISe, and core/shell CZISe/ZnS NCs with corresponding bulk reference structures of CISe (C35-1349) and In_2Se_3 (C20-494) from the JCPDS-ICDD.

chloride ions, playing an important role in the nucleation and growth of many types of NCs.[54] Here, the preferential attachment of the amine on the NC basal facets prevents their growth in the thickness direction.[17]

The subsequent step involved the addition of a small amount of the Cu-precursor, leading to the formation of In-rich CISe seeds, accompanied by a color change from bright yellow to brown, indicating the successful transformation. The reaction mixture was kept under stirring overnight to incorporate as much Cu^+ as possible into the In_2Se_3 seeds. Next, the temperature was raised to 215–240 °C, thus promoting the growth of the triangular NCs *via* recrystallization or oriented attachment of the seeds. Subsequent addition of DDT improved the colloidal stability of the CISe NCs formed. Afterwards, Zn^{2+} was incorporated into the CISe NCs *via* a partial CE, forming an alloyed quaternary CZISe composition. In the last step, the CZISe NCs were overgrown with a ZnS shell at 200 °C by employing Zn oleate and S dissolved in ODE as precursors.

From TEM images of CISe NCs grown at 240 °C depicted in Fig. S2,† we observe that the incorporation of Cu^+ leads to a significant change in their morphology, as compared to the In_2Se_3 nanosheets (Fig. S1†). In particular, the CISe particles grew much smaller and adopted a triangular shape. Furthermore, they seem to have formed stacks made of several platelets, as suggested by high-resolution TEM imaging (Fig. S2b and c†). This stacking of the NPLs could be attributed to the use of a single ligand, which leads to an ordered ligand arrangement, resulting in a lower solubility of the particles, as compared to a disordered ligand arrangement adopted in the case of a mixture of ligands.[32,55] The HAADF-STEM images (which mainly reflect atomic-number contrast) shown in Fig. S3a and S4a† further confirm that the main building blocks of the NCs are triangularly shaped NPLs. A few hexagons are observed as well. The EDXS-based element distribution maps presented in Fig. S3b† reveal a uniform distribution of Cu and Se, while the In distribution varies slightly, especially at the particle edges.

CISe generally exists in two crystalline phases – the tetragonal phase (low-temperature phase) and the cubic phase (high-temperature phase).[34] CISe NCs in the low-temperature

NPLs recently developed by our group.[32] The synthesis of the core CZISe NCs was carried out using a similar seed-mediated approach depicted in Fig. 1. A simple replacement of the S- with the Se-precursor in this procedure did not lead to a successful synthesis of 2D CISe and CZISe NCs. Therefore, it required a significant optimization of the reaction parameters. Generally, a high temperature and a long reaction time are favored to equilibrate the different reactivities of the S- and Se-precursors. In our approach, CISe NCs are grown from CISe seeds at a higher temperature followed by the incorporation of zinc to form quaternary CZISe particles. The first step involves the formation of In_2Se_3 seeds in OlAm, acting as a solvent and the ligand for the NCs, which also helps in breaking the symmetry and promotes their anisotropic growth, in addition to

tetragonal phase were reported by Tang et al.,[35] Zhong et al.,[34] and Bi et al.[37] Ultrathin hexagonal CISe NPLs obtained from tetragonal ungamite CuSe NPLs via CE were also reported for the first time by Berends et al.[36] In our case, CISe NCs crystallize in the tetragonal phase, as evidenced by their XRD pattern shown in Fig. 2. The positions of the reflections match well with the bulk tetragonal CISe reference (JCPDS card number C35-1349). The three pronounced reflections at 26.7°, 44.3°, and 52.6° correspond to the (112), (204), and (116) planes, respectively. However, the relative intensities of the NC reflections are significantly different compared to the bulk reference. The strong peak at 26.7° and lower-intensity peaks at 44.3° and 52.6° confirm the formation of the anisotropic NC structure growing mainly in the [112] direction. The lattice parameters calculated from the XRD patterns are as follows: $a = b = 0.577$ nm, $c = 1.158$ nm, which are in good agreement with the reported data ($a = b = 0.578$ nm, $c = 1.161$ nm).[34] The crystallite size, as calculated by the Scherrer equation, is

8.3 nm. It is worth noting that the addition of Cu triggers the crystallization of the CISe NCs in a different crystal structure compared to pure In$_2$Se$_3$ nanosheets. This alteration might be a plausible reason for their different morphologies.

In the next step, CISe NCs of three different sizes obtained at 215 °C, 230 °C, and 240 °C were treated with zinc 2-ethylhexanoate. As seen in Fig. 3a–c, at a higher reaction temperature the NPLs not only grow larger but also form quite uniform stacks built of several individual platelets. The HAADF-STEM image of the CZISe NCs presented in Fig. 3g and S4b† further confirms the triangular shape of their building blocks. EDXS-based element maps shown in Fig. 3h indicate the presence of Cu, In, and Se, whose distribution can be considered homogeneous, having in view a complex structure of the particles. The distribution of Zn, at the same time, is rather inhomogeneous with its location mainly on the particle surface, as a result of surface-limited CE reaction. Finally, after the shell growth, the NCs maintain their anisotropic triangular shape,
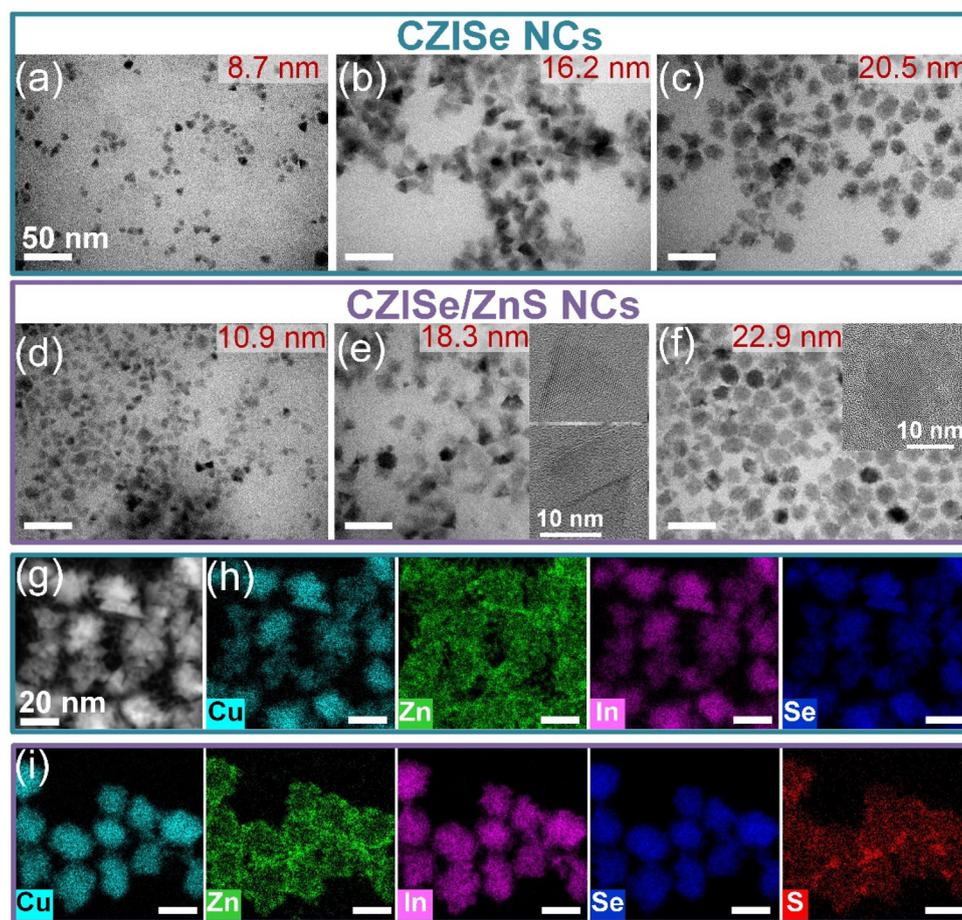

Fig. 3 TEM-based images of CZISe (a–c, g and h), and core/shell CZISe/ZnS (d–f and i) NCs of three different sizes (indicated in the images) synthesized using the corresponding CISe NCs grown at 215 °C, 230 °C, and 240 °C. Scale bars in (a–f) are 50 nm. Insets in (e) and (f) are high-resolution TEM (HRTEM) images of single CZISe/ZnS NCs, showing their triangular shape in (e) and stacking of triangular NPLs in (f). HAADF-STEM image of triangular stacked CZISe NCs (g) and corresponding EDXS-based element distribution maps (h) of Cu, Zn, In, and Se. EDXS-based element distribution maps of Cu, Zn, In, Se, and S in core/shell CZISe/ZnS NCs (i).

as seen in Fig. 3d–f. Element mapping reveals that in the core/shell NCs, Cu, In, and Se are located in the core region, while S is concentrated in the shell (Fig. 3i). At the same time, Zn is distributed all over the heterostructure with its higher concentration in the shell, as expected.

All three types of the NCs, *i.e.* CISe, CZISe, and CZISe/ZnS, were further characterized by ICP-OES analysis to determine their chemical composition, the results of which are presented in Fig. 4 in the form of different element ratios: Cu : In, Cu : Zn, In : Zn, and Se : S. These ratios reflect the evolution of the NCs' composition after each synthesis step and allow us to select several trends. First of all, from the Cu : In ratios, we can see that the copper content in the CISe NCs is much larger than in the Cu : In : Se feed ratio (0.015 : 0.3 : 0.2), varying from 0.62 to 0.82, indicating an efficient incorporation of Cu^+ ions into the In_2Se_3 seeds and proving the high affinity between Cu (I) and Se that justifies the choice of a low Cu feed amount in the synthesis. This Cu : In ratio in small- and medium-sized CZISe NCs decreases upon the zinc incorporation and the shell growth, while in large NCs, it increases after the zinc incorporation and then decreases after the shell growth (reaching the same amount as in the starting CISe NCs). This observation suggests that in smaller NCs, the Cu^+-to-Zn^{2+} CE is more efficient than the In^{3+}-to-Zn^{2+} CE, whereas in larger NCs, this trend is opposite. The Cu : Zn ratio in the CZISe NCs increases with their size from 0.22 to 0.85, implying that zinc more efficiently replaces copper and indium in smaller NCs than in the larger ones. After the shell growth, as expected, the ratio strongly decreases for all sizes, revealing the successful deposition of the ZnS layer. The In : Zn ratio in the CZISe NCs is larger than the Cu : Zn ratio, indicating the formation of an In-rich composition. This ratio, as the Cu : Zn one, strongly

decreases after the shell growth. Finally, the Se : S ratio in the CZISe NCs shows that sulphur incorporation occurs during the Cu^+-to-Zn^{2+} CE due to the presence of DDT in the reaction mixture and the quite high reaction temperature of 230 °C, in accord with observations of Lox *et al.* on similar CZISe NCs.[9] The ratio is smaller (*i.e.* the sulphur content is larger) in smaller NCs due to their larger surface-to-volume ratio and the contribution of sulphur from DDT molecules on the surface. As expected, the Se : S ratio drops significantly after the shell growth, remains in the case of large NCs about 1 though, indicating the formation of a quite thin (as compared to the core size) ZnS shell.

The XRD pattern of the CZISe NCs depicted in Fig. 2 indicates that the incorporation of Zn^{2+} and the growth of the ZnS shell trigger no significant changes in their crystal structure, *i.e.*, the tetragonal crystal structure is preserved, which is generally observed in the case of CE. A slight shift of the Bragg reflections to larger angles is observed after the incorporation of Zn, which is explained by the contraction of lattice due to the smaller lattice constant of zinc blende ZnSe (5.67 Å) compared to chalcopyrite $CuInSe_2$ (5.78 Å), a typical process for similar zinc incorporation in all CIS and CISe NCs.[24] The same small shift is visible in the pattern of the CZISe/ZnS NCs, indicating the shell growth.

Optical properties of anisotropic CISe, CZISe, and CZISe/ZnS NCs

The progress of the reaction from the formation of In_2Se_3 seeds to the final anisotropic core/shell CZISe/ZnS NCs was monitored by absorption spectroscopy. As seen from the spectra presented in Fig. 5a, In_2Se_3 seeds exhibit a featureless absorption with the onset at approx. 400 nm and a small
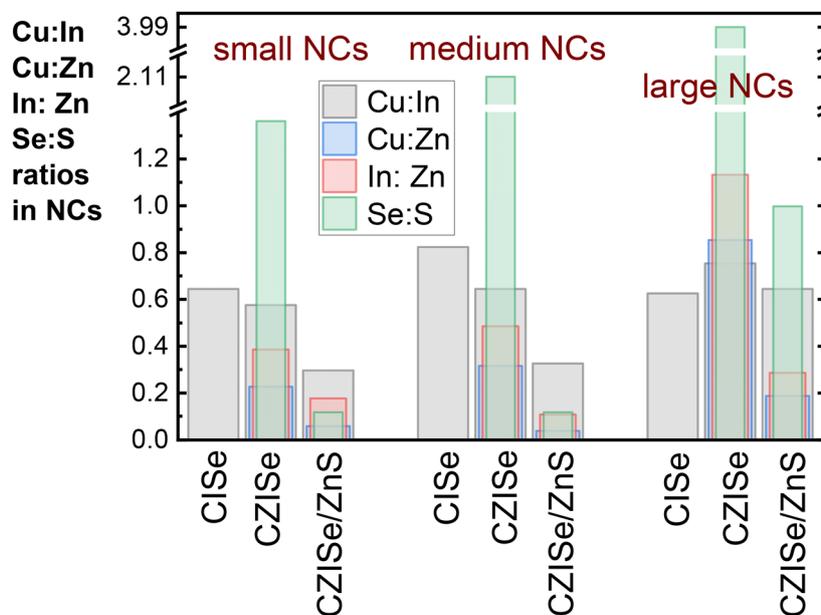

Fig. 4 Changes of the NCs' composition upon zinc incorporation and subsequent ZnS shell growth reflected by the corresponding element ratios: Cu : In, Cu : Zn, In : Zn, and Se : S.
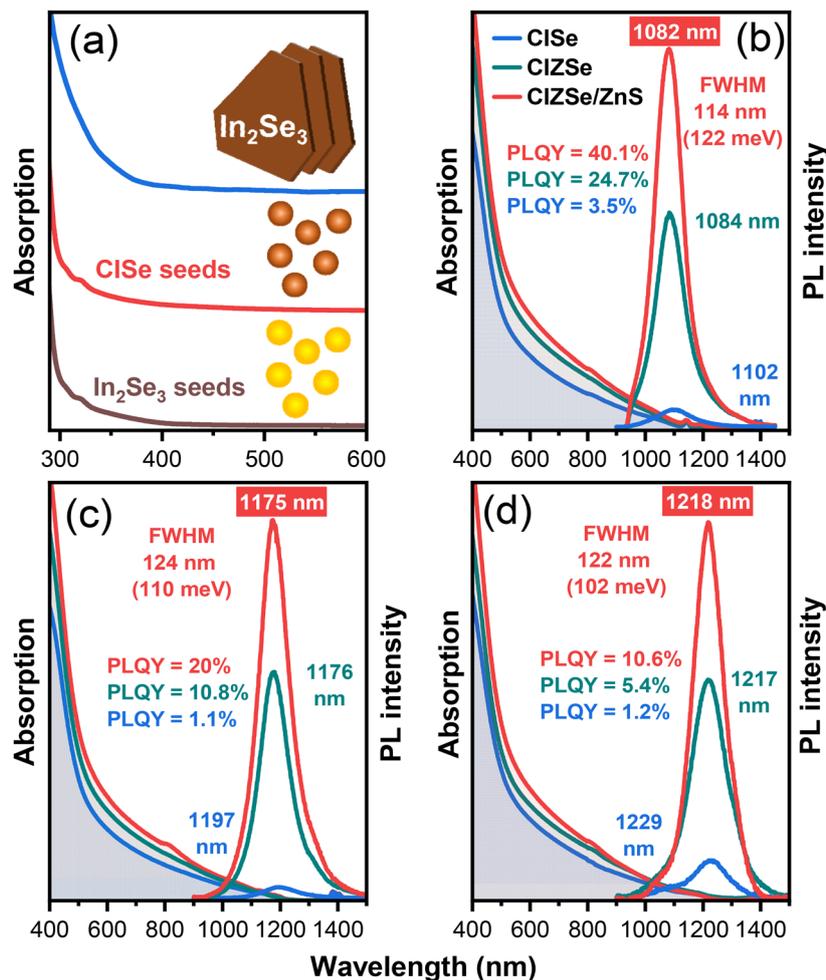
Fig. 5 Absorption spectra of In_2Se_3 seeds, CIS seeds, and In_2Se_3 nanosheets (a). Absorption and PL spectra of CISe, CZISe, and core/shell CZISe/ZnS NCs of three different sizes (small, medium, and large CZISe NCs – 8.7 nm, 16.2 nm, and 20.5 nm, respectively; small, medium, and large CZISe/ZnS NCs – 10.9 nm, 18.3 nm, and 22.9 nm, respectively), emitting with PL maxima at 1082 nm (b), 1175 nm (c), and 1218 nm (d) with corresponding PLQY and FWHM values.

shoulder at approx. 320 nm. In_2Se_3 nanosheets synthesized from the In_2Se_3 seeds also exhibit a featureless absorption. The incorporation of Cu^+ leading to the formation of CIS seeds triggers a slight red shift of the absorption onset. The formation of triangular CISe NCs accentuates the red shift due to the particle growth, resulting in the absorption onset at approx. 1160–1230 nm, whereas starting from approx. 500–550 nm, the absorption increases towards shorter wavelengths (Fig. 5b–d). After the addition of Zn^{2+} and subsequent ZnS shell growth, the absorption spectra undergo no significant changes in their shape, remaining mainly featureless, with the onset and the high short-wavelengths absorption region slightly shifting to shorter wavelengths. The shape of the spectra represents the commonly observed featureless absorption for CIS(Se)-based NCs. The origin of such a spectrum is most often attributed to the inhomogeneities in NC size, shape, and composition.[9] According to the TEM images, it is quite evident that these NCs are polydisperse in terms of their lateral sizes and likely differ in the composition of the individual NCs, thus leading to ensemble inhomogeneities and featureless absorption.

As a next step of the optical characterization, we acquired steady-state PL spectra of these NCs. CISe NCs of different compositions were emitting without the incorporation of zinc, however, the intensity of the PL was relatively low with PLQY values of about 1–3% (Fig. 5b–d). The PL spectra of the CISe NCs are tunable by varying the NCs' size in a quite narrow wavelength range: samples synthesized at 215 °C, 230 °C, and 240 °C exhibit PL maxima at 1102 nm, 1197 nm, and 1229 nm, respectively (Fig. 5b–d). We also monitored the growth of the CISe NCs over time and observed that with time, the intensity increased, and the maximum intensity was reached after 60 min of the growth (see Fig. S5a†). Decreasing the time of the Cu incorporation to 1 h led to a blue shift of the PL maximum along with a decrease in the PL intensity, as depicted in Fig. S5b.† Using a mixture of ligands to unstack the NPLs also led to a blue shift of the PL maximum accompanied by a considerable degradation of the PL inten-

sity, as seen in Fig. S5c.† Interestingly, a decreased amount of OlAm in the synthesis led to an increase of the PL intensity accompanied by a large blue shift of the PL maximum (Fig. S5d†). The blue shift of the PL maximum in these cases can be attributed to the decreased size of the NCs with different morphologies.

As follows from the PL spectra of the CZISe NCs, the incorporation of zinc led to a slight blue shift of the PL maximum along with a pronounced intensity enhancement. The shift of the PL maximum is commonly attributed to the enlarged band gap of the material, and a higher PL intensity than that of the CISe NCs is a result of the healing of crystallite defects, especially those on the surface *via* the formation of a ZnSe-rich shell.[56] We note that previously reported 3–5 nm CISe NCs emit between 600 nm and 800 nm with broad PL bandwidths of approx. 250 meV.[57,58] The dramatic red shift of the PL maxima of anisotropic CZISe NCs obtained in the present work can be attributed to the strong 1D quantum confinement, analogous to that observed in the case of thin CZIS NPLs.[32] The PLQY of the core CZISe NCs decreased from 24.7% through 10.8% to 5.4% upon shifting the PL maximum to longer wavelengths. The shell growth did not lead to a remarkable shift of the PL maximum position, indicating the absence of further Zn incorporation into the core. At the same time, it was accompanied by a two-fold enhancement of the PL intensity reaching a PLQY value as high as 40.1% for the sample emitting at 1082 nm (Fig. 5b).

Interestingly, our triangular stacked CZISe/ZnS NCs exhibit quite narrow bandwidths contrary to usually broad PL spectra inherent to this class of materials, which generally have full widths at half maximum (FWHM) values on the order of 300 meV.[59] This broadness of the PL has been established as an ensemble property of I–III–VI-based NCs by single particle studies, wherein PL bandwidths of single particles can be narrowed as compared to the PL bandwidth of the ensemble.[59,60] FWHM values determined for CZISe/ZnS NCs were 122 meV, 110 meV, and 102 meV for samples emitting at 1082 nm, 1175 nm, and 1218 nm, respectively (Fig. 5b–d). With apparently thin single CZISe triangles, much smaller than the exciton Bohr radius of CISe of 10.6 nm,[9] the resultant confinement in this direction is expected to be quite strong. The uniform thickness of these single CZISe triangles and the absence of compositional inhomogeneities are the probable reasons for this narrow NIR PL bandwidth. This makes the CZISe/ZnS NCs comparable emitters with PbSe NPLs possessing unprecedented narrow PL bandwidths as small as 70–80 meV[25] and ultrasmall $PbSe_xS_{1-x}$ NPLs with doubled FWHM values.[61] The generally accepted mechanism of the PL of I–III–VI-based NCs involves the radiative transition of a photoexcited electron to an intermediate state, originating from a Cu-defect (which can be either Cu^+ or Cu^{2+}), where it recombines with a residing hole.[62–65] A possible distribution of energies of these inter-gap states triggered by inhomogeneities of the NCs' size, shape, and composition results in a variation of the individual NC emission energies, leading to PL broadening. Nevertheless, the PL FWHM values achieved for the anisotropic CZISe/ZnS NCs in this work are by far the narrowest in this class of materials. The average lifetime determined from the time-resolved PL traces for the sample emitting at 1218 nm (Fig. S6†) is 98 ns for the CZISe NC core and 152 ns for the core/shell structure. These values are smaller than typically reported lifetimes on the order of hundreds of ns characteristic for this type of NCs,[32,66] indicating faster exciton recombination dynamics.

Conclusions

We report colloidal anisotropic CISe, CZISe, and core/shell CZISe/ZnS NCs synthesized in a one-pot seed-mediated approach. Those NCs synthesized at lower temperatures of 215 °C and 230 °C are single triangular particles, whereas the NCs grown at 240 °C constitute stacks containing several triangular particles overlaid on top of each other. Their anisotropic morphology is confirmed by HRTEM and HAADF-STEM imaging revealing triangular platelets. Both CISe and CZISe NCs adopt a tetragonal structure. The CISe NCs exhibit weak PL in the NIR range, while the incorporation of Zn leads to a significant enhancement of their PL intensity, which is further improved by the growth of a ZnS shell. The final heterostructured NCs exhibit an intensive PL with maxima ranging from 1082 nm to 1218 nm and PLQY reaching 40%. This is the first report of complex-shaped CISe-based NCs with inherent fluorescence. Along with this, the PL bands of the CZISe/ZnS NCs are, to the best of our knowledge, the narrowest so far reported for this class of materials, in the range of 102–122 meV. Thus, the synthetic strategy developed in this work contributes to the advancements in the field of anisotropic I–III–VI semiconductor nanomaterials along with significant improvement of their optical properties.

Author contributions

A. B., N. F., and A. S. contributed equally to this work.

Date availability

The data that support the findings of this study are available within the article and its ESI.† The raw data is available from the corresponding author upon reasonable request.

Conflicts of interest

There are no conflicts to declare.

Acknowledgements

References

1 S. A. McDonald, G. Konstantatos, S. Zhang, P. W. Cyr, E. J. D. Klem, L. Levina and E. H. Sargent, Solution-Processed PbS Quantum Dot Infrared Photodetectors and Photovoltaics, *Nat. Mater.*, 2005, **4**, 138–142.

2 O. T. Bruns, T. S. Bischof, D. K. Harris, D. Franke, Y. Shi, L. Riedemann, A. Bartelt, F. B. Jaworski, J. A. Carr, C. J. Rowlands, *et al.*, Next-Generation in Vivo Optical Imaging with Short-Wave Infrared Quantum Dots, *Nat. Biomed. Eng.*, 2017, **1**, 0056.

3 E. Hemmer, A. Benayas, F. Légaré and F. Vetrone, Exploiting the Biological Windows: Current Perspectives on Fluorescent Bioprobes Emitting above 1000 nm, *Nanoscale Horiz.*, 2016, **1**, 168–184.

4 Y. Ma, Y. Zhang and W. W. Yu, Near Infrared Emitting Quantum Dots: Synthesis, Luminescence Properties and Applications, *J. Mater. Chem. C*, 2019, **7**, 13662–13679.

5 T. T. Tan, S. T. Selvan, L. Zhao, S. Gao and J. Y. Ying, Size Control, Shape Evolution, and, Silica Coating of near-Infrared-Emitting PbSe Quantum Dots, *Chem. Mater.*, 2007, **19**, 3112–3117.

6 D. Deng, W. Zhang, X. Chen, F. Liu, J. Zhang, Y. Gu and J. Hong, Facile Synthesis of High–Quality, Water–Soluble, near–Infrared–Emitting PbS Quantum Dots, *Eur. J. Inorg. Chem.*, 2009, **23**, 3440–3446.

7 M. V. Kovalenko, E. Kaufmann, D. Pachinger, J. Roither, M. Huber, J. Stangl, G. Hesser, F. Schäffler and W. Heiss, Colloidal HgTe Nanocrystals with Widely Tunable Narrow Band Gap Energies: From Telecommunications to Molecular Vibrations, *J. Am. Chem. Soc.*, 2006, **128**, 3516–3517.

8 L. Yan, X. Shen, Y. Zhang, T. Zhang, X. Zhang, Y. Feng, J. Yin, J. Zhao and W. W. Yu, Near-Infrared Light Emitting Diodes Using PbSe Quantum Dots, *RSC Adv.*, 2015, **5**, 54109–54114.

9 J. F. L. Lox, Z. Dang, V. M. Dzhagan, D. Spittel, B. Martín-García, I. Moreels, D. R. T. Zahn and V. Lesnyak, Near-Infrared Cu–In–Se-Based Colloidal Nanocrystals via Cation Exchange, *Chem. Mater.*, 2018, **30**, 2607–2617.

10 A. Bora, J. Lox, R. Hübner, N. Weiß, H. Bahmani Jalali, F. Di Stasio, C. Steinbach, N. Gaponik and V. Lesnyak, Composition-Dependent Optical Properties of Cu–Zn–In–Se Colloidal Nanocrystals Synthesized via Cation Exchange, *Chem. Mater.*, 2023, **35**, 4068–4077.

11 P. M. Allen and M. G. Bawendi, Ternary I-III-VI Quantum Dots Luminescent in the Red to near-Infrared, *J. Am. Chem. Soc.*, 2008, **130**, 9240–9241.

12 O. Yarema, D. Bozyigit, I. Rousseau, L. Nowack, M. Yarema, W. Heiss and V. Wood, Highly Luminescent, Size- and Shape-Tunable Copper Indium Selenide Based Colloidal Nanocrystals, *Chem. Mater.*, 2013, **25**, 3753–3757.

13 H. McDaniel, A. Y. Koposov, S. Draguta, N. S. Makarov, J. M. Pietryga and V. I. Klimov, Simple yet Versatile Synthesis of $CuInSe_xS_{2-x}$ Quantum Dots for Sunlight Harvesting, *J. Phys. Chem. C*, 2014, **118**, 16987–16994.

14 Y. Jia, H. Liu, P. Cai, X. Liu, L. Wang, L. Ding, G. Xu, W. Wang, M. Jiao and X. Luo, Near-Infrared Emitting Cu-In-Se/ZnS Core/Shell Quantum Dots: Aqueous Synthesis and Sulfur Source Effects, *Chem. Commun.*, 2021, **57**, 4178–4181.

15 H. Liu, P. Cai, K. J. McHugh, C. F. Perkinson, L. Li, S. Wang, W. Wang, M. Jiao, X. Luo and L. Jing, Aqueous Synthesis of Bright Near-Infrared-Emitting Zn-Cu-In-Se Quantum Dots for Multiplexed Detection of Tumor Markers, *Nano Res.*, 2022, **15**, 8351–8359.

16 X. Tong, X.-T. Kong, Y. Zhou, F. Navarro-Pao, G. S. Selopal, S. Sun, A. O. Govorov, H. Zhao, Z. M. Wang and F. Rosei, Near-Infrared, Heavy Metal-Free Colloidal "Giant" Core/Shell Quantum Dots, *Adv. Energy Mater.*, 2018, **8**, 1701432.

17 A. C. Berends, J. D. Meeldijk, M. A. van Huis and C. de Mello Donega, Formation of Colloidal Copper Indium Sulfide Nanosheets by Two-Dimensional Self-Organization, *Chem. Mater.*, 2017, **29**, 10551–10560.

18 A. C. Berends and C. de Mello Donega, Ultrathin One- and Two-Dimensional Colloidal Semiconductor Nanocrystals: Pushing Quantum Confinement to the Limit, *J. Phys. Chem. Lett.*, 2017, **8**, 4077–4090.

19 M. Nasilowski, B. Mahler, E. Lhuillier, S. Ithurria and B. Dubertret, Two-Dimensional Colloidal Nanocrystals, *Chem. Rev.*, 2016, **116**, 10934–10982.

20 Y. Du, Z. Yin, J. Zhu, X. Huang, X. J. Wu, Z. Zeng, Q. Yan and H. Zhang, A General Method for the Large-Scale Synthesis of Uniform Ultrathin Metal Sulphide Nanocrystals, *Nat. Commun.*, 2012, **3**, 1177.

21 S. Ithurria, M. D. Tessier, B. Mahler, R. P. Lobo, B. Dubertret and A. L. Efros, Colloidal Nanoplatelets with Two-Dimensional Electronic Structure, *Nat. Mater.*, 2011, **10**, 936–941.

22 N. Kapuria, N. N. Patil, K. M. Ryan and S. Singh, Two-Dimensional Copper Based Colloidal Nanocrystals: Synthesis and Applications, *Nanoscale*, 2022, **14**, 2885–2914.

23 A. H. Khan, R. Brescia, A. Polovitsyn, I. Angeloni, B. Martín-García and I. Moreels, Near-Infrared Emitting Colloidal PbS Nanoplatelets: Lateral Size Control and Optical Spectroscopy, *Chem. Mater.*, 2017, **29**, 2883–2889.

24 J. F. L. Lox, Z. Dang, M. Lê Anh, E. Hollinger and V. Lesnyak, Colloidal Cu–Zn–In–S-Based Disk-Shaped Nanocookies, *Chem. Mater.*, 2019, **31**, 2873–2883.

25 T. Galle, M. Samadi Khoshkhoo, B. Martin-Garcia, C. Meerbach, V. Sayevich, A. Koitzsch, V. Lesnyak and A. Eychmüller, Colloidal PbSe Nanoplatelets of Varied Thickness with Tunable Optical Properties, *Chem. Mater.*, 2019, **31**, 3803–3811.

26 X. Tao, E. Mafi and Y. Gu, Synthesis and Ultrafast Carrier Dynamics of Single-Crystal Two-Dimensional $CuInSe_2$ Nanosheets, *J. Phys. Chem. Lett.*, 2014, **5**, 2857–2862.

27 C. Bouet, M. D. Tessier, S. Ithurria, B. Mahler, B. Nadal and B. Dubertret, Flat Colloidal Semiconductor Nanoplatelets, *Chem. Mater.*, 2013, **25**, 1262–1271.

28 E. Lhuillier, S. Pedetti, S. Ithurria, B. Nadal, H. Heuclin and B. Dubertret, Two-Dimensional Colloidal Metal Chalcogenides Semiconductors: Synthesis, Spectroscopy, and Applications, *Acc. Chem. Res.*, 2015, **48**, 22–30.

29 W.-k. Koh, N. K. Dandu, A. F. Fidler, V. I. Klimov, J. M. Pietryga and S. V. Kilina, Thickness-Controlled Quasi-Two-Dimensional Colloidal PbSe Nanoplatelets, *J. Am. Chem. Soc.*, 2017, **139**, 2152–2155.

30 Y. Liu, M. Liu and M. T. Swihart, Shape Evolution of Biconcave Djurleite $Cu_{1.94}S$ Nanoplatelets Produced from $CuInS_2$ Nanoplatelets by Cation Exchange, *J. Am. Chem. Soc.*, 2017, **139**, 18598–18606.

31 X.-J. Wu, X. Huang, X. Qi, H. Li, B. Li and H. Zhang, Copper-Based Ternary and Quaternary Semiconductor Nanoplates: Templated Synthesis, Characterization, and Photoelectrochemical Properties, *Angew. Chem., Int. Ed.*, 2014, **53**, 8929–8933.

32 A. Bora, A. Prudnikau, N. Fu, R. Hübner, K. B. L. Borchert, D. Schwarz, N. Gaponik and V. Lesnyak, Seed-Mediated Synthesis of Photoluminescent Cu–Zn–In–S Nanoplatelets, *Chem. Mater.*, 2022, **34**, 9251–9260.

33 V. Lesnyak, C. George, A. Genovese, M. Prato, A. Casu, S. Ayyappan, A. Scarpellini and L. Manna, Alloyed Copper Chalcogenide Nanoplatelets via Partial Cation Exchange Reactions, *ACS Nano*, 2014, **8**, 8407–8418.

34 H. Zhong, Y. Li, M. Ye, Z. Zhu, Y. Zhou, C. Yang and Y. Li, A Facile Route to Synthesize Chalcopyrite $CuInSe_2$ Nanocrystals in Non-Coordinating Solvent, *Nanotechnology*, 2007, **18**, 025602.

35 J. Tang, S. Hinds, S. O. Kelley and E. H. Sargent, Synthesis of Colloidal $CuGaSe_2$, $CuInSe_2$, and $Cu(InGa)Se_2$ Nanoparticles, *Chem. Mater.*, 2008, **20**, 6906–6910.

36 A. C. Berends, W. van der Stam, Q. A. Akkerman, J. D. Meeldijk, J. van der Lit and C. de Mello Donega, Anisotropic 2D $Cu_{2-x}Se$ Nanocrystals from Dodecaneselenol and Their Conversion to CdSe and $CuInSe_2$ Nanoparticles, *Chem. Mater.*, 2018, **30**, 3836–3846.

37 W. Bi, M. Zhou, Z. Ma, H. Zhang, J. Yu and Y. Xie, $CuInSe_2$ Ultrathin Nanoplatelets: Novel Self-Sacrificial Template-Directed Synthesis and Application for Flexible Photodetectors, *Chem. Commun.*, 2012, **48**, 9162–9164.

38 Q. A. Akkerman, A. Genovese, C. George, M. Prato, I. Moreels, A. Cabot, S. Marras, A. Curcio, A. Scarpellini, T. Pellegrino, *et al.*, From Binary Cu_2S to Ternary Cu-In-S and Quaternary Cu-In-Zn-S Nanocrystals with Tunable Composition via Partial Cation Exchange, *ACS Nano*, 2015, **9**, 521–531.

39 B. J. Beberwyck, Y. Surendranath and A. P. Alivisatos, Cation Exchange: A Versatile Tool for Nanomaterials Synthesis, *J. Phys. Chem. C*, 2013, **117**, 19759–19770.

40 L. De Trizio and L. Manna, Forging Colloidal Nanostructures via Cation Exchange Reactions, *Chem. Rev.*, 2016, **116**, 10852–10887.

41 V. Lesnyak, Chemical Transformations of Colloidal Semiconductor Nanocrystals Advance Their Applications, *J. Phys. Chem. Lett.*, 2021, **12**, 12310–12322.

42 V. Lesnyak, R. Brescia, G. C. Messina and L. Manna, Cu Vacancies Boost Cation Exchange Reactions in Copper Selenide Nanocrystals, *J. Am. Chem. Soc.*, 2015, **137**, 9315–9323.

43 S. Vikulov, F. Di Stasio, L. Ceseracciu, P. L. Saldanha, A. Scarpellini, Z. Dang, R. Krahne, L. Manna and V. Lesnyak, Fully Solution-Processed Conductive Films Based on Colloidal Copper Selenide Nanosheets for Flexible Electronics, *Adv. Funct. Mater.*, 2016, **26**, 3670–3677.

44 V. Shamraienko, D. Spittel, R. Hübner, M. Samadi Khoshkhoo, N. Weiß, M. Georgi, K. B. L. Borchert, D. Schwarz, V. Lesnyak and A. Eychmüller, Cation Exchange on Colloidal Copper Selenide Nanosheets: A Route to Two-Dimensional Metal Selenide Nanomaterials, *J. Mater. Chem. C*, 2021, **9**, 16523–16535.

45 H. Migge and J. Grzanna, Thermochemistry in the System Cu–In–S at 723 K, *J. Mater. Res.*, 2011, **9**, 125–131.

46 B. Chen, S. Chang, D. Li, L. Chen, Y. Wang, T. Chen, B. Zou, H. Zhong and A. L. Rogach, Template Synthesis of $CuInS_2$ Nanocrystals from In_2S_3 Nanoplates and Their Application as Counter Electrodes in Dye-Sensitized Solar Cells, *Chem. Mater.*, 2015, **27**, 5949–5956.

47 Z. Yuan, L. Yang, D. Han, G. Sun, C. Zhu, Y. Wang, Q. Wang, M. Artemyev and J. Tang, Synthesis and Optical Properties of In_2S_3-Hosted Colloidal Zn-Cu-In-S Nanoplatelets, *ACS Omega*, 2021, **6**, 18939–18947.

48 K. H. Park, K. Jang and S. U. Son, Synthesis, Optical Properties, and Self-Assembly of Ultrathin Hexagonal In_2S_3 Nanoplates, *Angew. Chem., Int. Ed.*, 2006, **45**, 4608–4612.

49 A. Saha, R. Yadav, D. Aldakov and P. Reiss, Gallium Sulfide Quantum Dots with Zinc Sulfide and Alumina Shells Showing Efficient Deep Blue Emission, *Angew. Chem., Int. Ed.*, 2023, **62**, e202311317.

50 L. Liu, J. Dong, J. Huang, A. Nie, K. Zhai, J. Xiang, B. Wang, F. Wen, C. Mu, Z. Zhao, *et al.*, Atomically Resolving Polymorphs and Crystal Structures of In_2Se_3, *Chem. Mater.*, 2019, **31**, 10143–10149.

51 X. Tao and Y. Gu, Crystalline-Crystalline Phase Transformation in Two-Dimensional In_2Se_3 Thin Layers, *Nano Lett.*, 2013, **13**, 3501–3505.

52 J. Li, H. Li, X. Niu and Z. Wang, Low-Dimensional In_2Se_3 Compounds: From Material Preparations to Device Applications, *ACS Nano*, 2021, **15**, 18683–18707.

53 G. Almeida, S. Dogan, G. Bertoni, C. Giannini, R. Gaspari, S. Perissinotto, R. Krahne, S. Ghosh and L. Manna, Colloidal Monolayer β-In₂Se₃ Nanosheets with High Photoresponsivity, *J. Am. Chem. Soc.*, 2017, **139**, 3005–3011.

54 S. Ghosh and L. Manna, The Many "Facets" of Halide Ions in the Chemistry of Colloidal Inorganic Nanocrystals, *Chem. Rev.*, 2018, **118**, 7804–7864.

55 Y. Yang, H. Qin and X. Peng, Intramolecular Entropy and Size-Dependent Solution Properties of Nanocrystal-Ligands Complexes, *Nano Lett.*, 2016, **16**, 2127–2132.

56 W. Guo, N. Chen, Y. Tu, C. Dong, B. Zhang, C. Hu and J. Chang, Synthesis of Zn-Cu-In-S/ZnS Core/Shell Quantum Dots with Inhibited Blue-Shift Photoluminescence and Applications for Tumor Targeted Bioimaging, *Theranostics*, 2013, **3**, 99–108.

57 S. Qu, X. Yuan, Y. Li, X. Li, X. Zhou, X. Xue, K. Zhang, J. Xu and C. Yuan, Aqueous Synthesis of Composition-Tuned Defects in CuInSe₂ Nanocrystals for Enhanced Visible-Light Photocatalytic H₂ Evolution, *Nanoscale Adv.*, 2021, **3**, 2334–2342.

58 H. Zhong, Z. Wang, E. Bovero, Z. Lu, F. C. J. M. van Veggel and G. D. Scholes, Colloidal CuInSe₂ Nanocrystals in the Quantum Confinement Regime: Synthesis, Optical Properties, and Electroluminescence, *J. Phys. Chem. C*, 2011, **115**, 12396–12402.

59 H. Zang, H. Li, N. S. Makarov, K. A. Velizhanin, K. Wu, Y. S. Park and V. I. Klimov, Thick-Shell CuInS₂/ZnS Quantum Dots with Suppressed "Blinking" and Narrow Single-Particle Emission Line Widths, *Nano Lett.*, 2017, **17**, 1787–1795.

60 P. J. Whitham, A. Marchioro, K. E. Knowles, T. B. Kilburn, P. J. Reid and D. R. Gamelin, Single-Particle Photoluminescence Spectra, Blinking, and Delayed Luminescence of Colloidal CuInS₂ Nanocrystals, *J. Phys. Chem. C*, 2016, **120**, 17136–17142.

61 Y. Zhou, M. Celikin, A. Camellini, G. Sirigu, X. Tong, L. Jin, K. Basu, X. Tong, D. Barba, D. Ma, S. Sun, F. Vidal, M. Zavelani-Rossi, Z. M. Wang, H. Zhao, A. Vomiero and F. Rosei, Ultrasmall Nanoplatelets: The Ultimate Tuning of Optoelectronic Properties, *Adv. Energy Mater.*, 2017, **7**, 1602728.

62 M. V. Kovalenko, L. Manna, A. Cabot, Z. Hens, D. V. Talapin, C. R. Kagan, V. I. Klimov, A. L. Rogach, P. Reiss, D. J. Milliron, *et al.*, Prospects of Nanoscience with Nanocrystals, *ACS Nano*, 2015, **9**, 1012–1057.

63 A. C. Berends, F. T. Rabouw, F. C. Spoor, E. Bladt, F. C. Grozema, A. J. Houtepen, L. D. Siebbeles and C. de Mello Donega, Radiative and Nonradiative Recombination in CuInS₂ Nanocrystals and CuInS₂-Based Core/Shell Nanocrystals, *J. Phys. Chem. Lett.*, 2016, **7**, 3503–3509.

64 A. Fuhr, H. J. Yun, S. A. Crooker and V. I. Klimov, Spectroscopic and Magneto-Optical Signatures of Cu^{1+} and Cu^{2+} Defects in Copper Indium Sulfide Quantum Dots, *ACS Nano*, 2020, **14**, 2212–2223.

65 D. H. Jara, K. G. Stamplecoskie and P. V. Kamat, Two Distinct Transitions in Cu_xInS_2 Quantum Dots. Bandgap Versus Sub-Bandgap Excitations in Copper-Deficient Structures, *J. Phys. Chem. Lett.*, 2016, **7**, 1452–1459.

66 L. De Trizio, M. Prato, A. Genovese, A. Casu, M. Povia, R. Simonutti, M. J. P. Alcocer, C. D'Andrea, F. Tassone and L. Manna, Strongly Fluorescent Quaternary Cu–In–Zn–S Nanocrystals Prepared from $Cu_{1-x}InS_2$ Nanocrystals by Partial Cation Exchange, *Chem. Mater.*, 2012, **24**, 2400–2406.